Mineralogical Magazine (2021), **85**, 708–715
doi:10.1180/mgm.2021.66

CAMBRIDGE UNIVERSITY PRESS

Article

Synthesis and structure of calumetite-like $SrCu_4(OH)_8Cl_2{\cdot}3.5H_2O$

Wilson A. Crichton[1]*, Harald Müller[1] and Matteo Leoni[2]

[1]ESRF- The European Synchrotron, 71 avenue des Martyrs, 38000 Grenoble, France; and [2]Saudi Aramco R&D Center, PO BOX 62, 31311 Dhahran, Saudi Arabia

Abstract

The synthesis and structure of the title compound, **1**, is presented, refined using Rietveld against powder X-ray diffraction data. **1** crystallises dominantly in a pseudotetragonal *C*-centred orthorhombic lattice with dimensions $a = 6.6791(6)$ Å, $b = 15.5006(6)$ Å, $c = 6.6811(6)$ Å and $V = 691.70(10)$ Å^3. The structural model proposed here refined by Rietveld is $Sr_{0.928(8)}Cu_4(OH)_8Cl_2{\cdot}3.60(21)H_2O$ in space group *Cmcm* (63), with $Z = 2$. The chemistry and diffraction pattern of **1** are similar to that for the known Ca analogue, calumetite. The copper sites are arranged with square planar coordination at ¼ and ¾ height and are bonded to four (protonated) oxygens at an average of 1.966 Å (effective coordination of 3.82 Å). The more distant Cl sites (at Cu−Cl = 3.190(6) Å) complete the heavily Jahn–Teller distorted $Cu[(OH)_4,Cl_2]$ polyhedra. The ½-occupied Sr sites are 8 coordinated to four protonated oxygens shared with the Cu-layer (at $2 \times 2.438(8)$ Å, $2 \times 2.566(15)$ Å) and by 4 bonds to the proposed water sites (Sr−Ow = 2.760(9) Å). The structure of **1** is predisposed towards defects, based on a notional tetragonal, *P4/nmm*, substructure with $a_{sub} \approx a_1$, $c_{sub} = b_{½}$ dimensions. Average diffraction models have been further elaborated in order to resolve additional peaks (and peak-shapes) using *DIFFaX+*.

Keywords: calumetite, atacamite, kapellasite, structure, diffraction, synthesis

(Received 5 May 2021; accepted 19 August 2021; Accepted Manuscript published online: 17 September 2021; Associate Editor: Daniel Atencio)

Introduction

Basic copper hydroxychloride salts are of much interest to a wide variety of researchers; in fields ranging from the development and use of fungicides (e.g. for the treatment of peronospora in vineyards) to those investigating frustrated magnetism. The description of the synthesis of a whole range of compositions, most notably by Feitknecht and co-workers, (Feitknecht, 1949; Oswald and Feitknecht, 1964) are continued and extended today – at an industrial scale for some particular compositions. Erdös *et al.* (1981) have described in detail a series of (partly) hydrated basic copper hydroxychlorides that form at moderate temperatures through the corrosion of copper held at increasing temperatures in NH_3-containing and oxygenated aqueous solutions of $CaCl_2$. One of these, described as $4Cu(OH)_2{\cdot}CaCl_2{\cdot}3.5H_2O$, was estimated as tetragonal with at least a $P4_2$ symmetry and lattice of $a = 9.392$ and $c = 15.077$ Å, and was compared by Erdös *et al.* to the calumetite of Williams (1963). It was also observed to dehydrate via a complex sequence of further hydroxychloride phases. Another phase is described as rehydrating in a hexagonal lattice with composition $3Cu(OH)_2{\cdot}CaCl_2{\cdot}H_2O$, with $a = 6.66$ Å and $c = 5.81$ Å. This latter phase has been isolated synthetically and described, from natural samples, as centennialite, a relative of the kapellasite family (Crichton and Müller, 2017). The synthesis of single crystals has been further elaborated (Sun *et al.*, 2016), which has also afforded more detailed structural analysis at 213 K, to a noncentrosymmetric *P3m*1 with disordered Ca positions (Yoshida *et al.*, 2017). Centennialite, thus proposed, has a chemistry and lattice essentially as described by Erdös *et al.* and is, as are the kapellasites in general, a trigonal phase that exhibits the same 2-dimensional Kagome pattern of planar 4-coordinated Cu sites separated by M^{2+} polyhedra much desired by investigators of frustrated magnetism, but more particularly in this case due to the significant mismatch between the ionic radii of the divalent cations, which limits site intermixing.

As part of their same study, Crichton and Müller also synthesised a composition that was identical to the initial phase of Erdös *et al.*, with a composition of $CaCu_4(OH)_8Cl_2{\cdot}3.5H_2O$ and demonstrated that a centennialite could be obtained from it by heating, which reflected the measurements made previously upon their synthetic counterparts (Erdös *et al.*, 1981). The solution of that structure led to a proposition for a calumetite model that matched a variety of data from various sources, including those newly collected from Williams (1963) actual samples. Similar phases were also isolated by Lubej *et al.* (2004) during optimisation of the synthetic processes involved in the production of Cuprablau-Z. Crichton and Müller's structural description led them to further propose a topological relationship between their proposed calumetite structure and the kapellasite-like centennialite. In doing so they generated a structural motif, which reduces to the tetragonal lattice shared by Erdös *et al.*'s observed intermediate hemihydrate. The structural similarity between these phases prompted Erdös *et al.* to promote topotaxy and pseudomorphosis in the sequence of phases observed. Williams' calumetite has since been redefined with the formula to include essential Ca, as $CaCu_4(OH)_8Cl_2{\cdot}3.5H_2O$ (Miyawaki *et al.*, 2019). This is in line with the expectations from the synthetic compound of Erdös *et al.*, and the models refined against Williams' samples by Crichton and Müller. This consequently discredited 'vondechenite' (Schlüter *et al.*, 2019) as identical to the pre-existing calumetite. The single-crystal results obtained by those authors were

*Author for correspondence: Wilson A. Crichton, Email: crichton@esrf.fr
Cite this article: Crichton W.A., Müller H. and Leoni M. (2021) Synthesis and structure of calumetite-like $SrCu_4(OH)_8Cl_2{\cdot}3.5H_2O$. *Mineralogical Magazine* **85**, 708–715. https://doi.org/10.1180/mgm.2021.66

Table 1: Results of the synthesis of atacamite and kapellasite-like compounds using compressed air as oxidant.

Metal salt	Reaction time [h]	Reaction temp. [°C]	Mineral type	Comments	Elemental analysis, wt.% obs (calc) M^{2+}, Cu, O, Cl, H	LSQ M^{2+}:Cu, at. per 6 OH, balanced by OH
$CaCl_2 \cdot 2H_2O$*	3	85	Centennialite		Crichton and Müller (2017)	
$MgCl_2 \cdot 6H_2O$*	9	40	Haydeeite + Tondiite	Blue reaction mixture blue still contains lots of unreacted Cu	n.d., obvious mixture by diffraction	
$ZnCl_2$**	3	85	Clinoatacamite		18.5 (15.2), 40.4 (44.4), n.d. (23.4), 16.9 (16.5), 1.46 (1.41)	1.22:2.70
$CdCl_2 \cdot 2.5H_2O$**	3	85	Clinoatacamite-(Cd)		26.6 (23.6), 36.7 (40.0), n.d. (20.2), 14.1 (14.9), n.d. (1.27)	1.17:2.78
$NiCl_2 \cdot 6H_2O$**	3	85	Clinoatacamite-(Ni)	Excess H in separate assay (1.75 wt.%)	19.7 (13.9), 37.0 (38.2), n.d. (25.2), 16.6 (16.7), n.d. (1.59)	1.47:2.51
$CoCl_2 \cdot 6H_2O$**	3	85	Leverettite		16.3 (13.9), 41.4 (45.4), n.d. (22.7), 16.3 (16.8), n.d. (1.43)	1.20:2.76
$MnCl_2 \cdot 4H_2O$**	3	85	Misakiite		14.5 (13.1), 44.3 (45.6), 21.2 (22.9), 16.2 (16.9), 1.5 (1.44)	1.09:2.93

*Reaction conditions: Cu (µm-sized powder for organic synthesis or turnings; 1 g), metal chloride (0.5 M solution; 200 ml) with aqueous ammonia solution added (33 mass-%), reaction temperature corresponds to oil-bath temperature, 500 ml washing bottle; Drechsel insert (Por. 1); compressed air.
**Reaction conditions identical to those described before, but without addition of ammonia solution.

Table 2. Results of the synthesis of atacamite and kapellasite-like compounds using oxygen as oxidant.

Metal Salt	Reaction time [h]	Reaction Temp. [°C]	Mineral type	Comments
$ZnCl_2$*	2.5	25	Kapellasite	
$ZnCl_2$*	3.5	90	Kapellasite	
$MgCl_2 \cdot 6H_2O$** NH_3 (1ml)	4	40	Haydeeite + Tondiite	Reaction occurs only after addition of ammonia
$MnCl_2 \cdot 4H_2O$**	2.5	25, then 85	Misakiite	Mint-green powder, 3 g
$SrCl_2 \cdot 6H_2O$** NH_3 (1ml) + 10ml	5	40	Calumetite	Blue-grey powder
$SrCl_2 \cdot 6\ H_2O$** NH_3 (5 ml) + 10ml	5	40	Calumetite***	Two products: bright-blue solid 1.135g; brownish solid 0.3 g
$SrCl_2 \cdot 6H_2O$** NH_3 (5 ml) + 10ml	7	65	Calumetite****	Centrifuged; blue-grey powder; 1.924 g

*Reaction conditions: Cu (µm-sized powder for organic synthesis or turnings; 1 g), metal chloride (0.5 M solution; 200 ml) reaction temperature corresponds to oil-bath temperature, 500 ml washing bottle; Drechsel insert; oxygen.
**Addition of aqueous ammonia solution (33 mass-%) as indicated.
***Elemental analysis gives: 13.6 (calculated 13.8) wt.% Sr, 42.5 (40.0) Cu, 27.3 (29.0) O, 10.6 (11.2) Cl, 2.41 (2.38) H. This reduces to a charge-constrained stoichiometry $Sr_{0.91}Cu_{4.15}(O_{1.00}H_{1.008})_{8.00}Cl_{2.29} \cdot 3.50H_2O$.
****For elemental analysis data see text.

coincident to the structure presented in Crichton and Müller's table 6 and identical to the composition of the material produced by Erdös *et al.* (1981).

In an investigation of the wider utility of the same synthetic protocol used for the synthesis of the Ca-essential compounds (Tables 1–2), we have successfully produced synthetic equivalents to various kapellasites: Zn, $a = 6.31468(10)$ Å and $c = 5.72310(19)$ Å (cf. $a = 6.300(1)$ Å and $c = 5.733(1)$ Å, kapellasite; Krause *et al.*, 2006); Mg, $a = 6.27815(23)$ Å and $c = 5.7595(5)$ Å (cf. $a = 6.2733(4)$ Å and $c = 5.7472(5)$ Å, haydeeite; Malcherek and Schlüter, 2007); Mn, $a = 6.42533(17)$ Å and $c = 5.71048(11)$ Å (cf. $a = 6.4168(4)$ Å and $c = 5.7099(4)$ Å, misakiite; Nishio-Hamane *et al.*, 2017), centennialite, calumetite (and both together), Crichton and Müller (2017); clinoatacamite-like: Cd, with $a = 6.3889(10)$ Å, $b = 7.05329(11)$ Å, $c = 9.3378(11)$ Å and $\beta = 99.034(15)°$ (e.g. McQueen *et al.*, 2011); Ni, with $a = 6.1746(6)$ Å, $b = 6.8821(5)$ Å, $c = 9.0308(7)$ Å and $\beta = 99.46(8)°$ and rhombohedral forms: Co, with $a = 6.8476(4)$ Å and $c = 14.1382(22)$ Å (cf. $a = 6.8436(6)$ Å and $c = 14.0637(10)$ Å, leverettite; Kampf *et al.*, 2013); Zn, $a = 6.85427(10)$ Å and $c = 14.1387(5)$ Å (cf. $a = 6.834(1)$ Å and $c = 14.075(2)$ Å herbertsmithite; Braithwaite *et al.*, 2004); Mg, with $a = 6.8397(6)$ and $c = 13.952(3)$ Å (cf. $a = 6.8345(2)$ Å and $c = 14.0022(7)$ Å, tondiite; Malcherek *et al.*, 2014). In addition, attempted reactions with Ba, Li, Na and K failed and produced tenorite (+/- witherite, possibly through reaction with entrained $(NH_4)_2CO_3$). Similarly, the use of mercury(II) chloride yielded calomel, Hg_2Cl_2, instead of any obvious discrete Cu precipitate. No atacamites or botallackites were produced. Interestingly, the M^{2+} = Sr run produced another calumetite-like phase which has not been described previously from Nature or synthesis. It has demonstrably the same structure as the Ca-essential phase and it is the fuller description of this phase that forms this manuscript. A centennialite equivalent has not yet been identified, but, given the increased discordance between the ionic radii of Cu^{2+} and Sr^{2+}, it too should go beyond the magnetic properties presented by the kapellasites, by excluding the potential for site intermixing (e.g. Iida *et al.*, 2020, Yoshida *et al.*, 2017). The failure of the Ba (Hg is rather different) and Cd compositions may indicate limits, for

https://doi.org/10.1180/mgm.2021.66 Published online by Cambridge University Press

example based on ionic radii, to formation of calumetite-like phases; leaving Pb (we recall that murdochite that shares very similar topological features; e.g. Dubler *et al.*, 1983) and some select lanthanoids as the remaining contenders.

Synthesis

Copper powder (1 g; 0.0157 mol; µm-sized powder for organic synthesis) was transferred into a washing bottle (500 ml), then solutions of strontium chloride hexahydrate (53.32 g; 0.2 mol) in demineralised water (200 ml) and aqueous ammonia (for detailed reaction conditions see Table 2) were added.

The reaction mixture was heated with stirring, then oxygen was passed through with the help of a standard Drechsel insert. Efficient mixing was assured by vigorous bubble-stirring as well as magnetic agitation. The colour of the reaction mixture changed gradually from colourless to blue-grey, RHS 119C, accompanied by the formation of a thick slurry, while the suspended copper particles disappeared gradually. After a reaction time of 4 h, additional aqueous ammonia (10 ml; 33 mass-% of NH_3) was added. Gas-bubbling and heating was continued for a period of 2 h.

After cooling to ambient temperature, the blue-grey product was collected on a Büchner funnel, rinsed with water (3 × 10 ml), EtOH abs. (2 × 10 ml) and Et_2O (2 × 10 ml), and dried over silica gel. The yield was 1.95 g (20% based on Cu) of a blue-grey powder. The infrared (IR) spectra, collected on a Specac Golden Gate ATR device, identified the following bands (vs = very strong): ν = 3609, 3425, 3303, 3146 (vs), 1613, 1299, 1190, 900 (vs), 723 cm^{-1}.

Chemistry

Quantitative chemical analyses of all elements present were performed by Mikroanalytisches Labor Pascher, Remagen, Germany. The data calculated for $SrCu_4(OH)_8Cl_2{\cdot}3.5H_2O$ (611.7 g/mol) were (wt.%): H 2.47, O 30.06, Cl 11.59, Sr 14.32 and Cu 41.55. Measured data were: H 2.39 (2.41), O 30.37 (30.37), Cl 11.4 (11.5), Sr 14.4 (14.4) and Cu 41.2 (41.4), where values in parentheses refer to the result of independent double determinations (Table 2; batch CuSrOx 60/1). Estimations (provided by the same laboratory) of the absolute experimental errors of the various analytical processes involved are: H 0.1 mass% (by IR spectroscopy on water following combustion in oxygen flow); Cl^- 0.2 mass% (by ion chromatography, following dissolution in H_2O/HNO_3); O 1 mass% (by hot wire detection of CO, following burning in carbon and chromatographic gas separation), and Cu and Sr, 1 and 0.2 mass%, respectively (both by inductively coupled plasma atomic emission spectroscopy following dissolution in hydrochloric acid).

Data collection and refinement

The recovered sample was placed into a 0.9 mm glass capillary and mounted on a sample spinner at ID31, ESRF, where ADX data were collected at λ = 0.3999(1) Å (Fitch, 2004). Given the evident similarity of **1** with calumetite and Erdös *et al.*'s phase, the model was refined with initial coordinates given by Crichton and Müller (2017), in *Cmcm*. The resulting refinement, in *Jana2006* (Petříček *et al.*, 2014), given in Tables 3,4 and Fig. 1, reproduces the expected calumetite-like model, which has been compared previously (Crichton and Müller, 2017; Schlüter *et al.*, 2019) to the rhenate of Jarek *et al.* (2007). Structural elements also share similar structural features with centennialite; e.g. Cu–Sr–Cu angles ~60° (here, 58.23(9)°). The characteristic array of Cu–OH planar polyhedra, with average length of 1.965 Å, form the equatorial bonds in the highly Jahn–Teller distorted octahedra (distortion at 0.2291, quadratic elongation at 1.1224), capped by the weak apical Cu–Cl of 3.190(5) Å (Table 5). The Sr[2OH, 2OH, $4H_2O$] square antiprisms are more regular (distortion of 0.049) with the four weaker 2.760(9) Å bonds to the water molecule at Ow and 2+2 to the bridging oxygens between the four surrounding Cu polyhedra, at 2× 2.434(7) and 2× 2.567(14) Å. While the Cu–Cl bond is weaker than in comparable atacamites, the pyramidal Ow–(H2)···Cl distance is remarkably strong and regular. Each Ow is coordinated in a tetrahedral arrangement to two Sr (2.760(8) Å) and two Cl (2.908(9) Å), with a low distortion of 0.02 and elongation of 1.006, and these form an infinite edge-sharing mackinawite-like sheet. Such a bonding environment, and the H-bonding scheme that will decorate it, is anticipated to provide considerable strength to this water-rich 'layer'. This model was subsequently imported to *Endeavour* (Putz *et al.*, 1999) for attempted location of H sites. This progressed in two stages; 16H were added to a fully charged and occupied fixed structure, which, in 80% of tests located potential water positions on a 16*h* position at, on average, (0.282, 0.043, 0.060) and is analogous to the part-occupied water position in centennialite, being coordinated by the Sr polyhedron. They also mirror those of CaCl $(ReO_4){\cdot}4H_2O$ (Jarek *et al.*, 2007), where they provide a water-rich layer that caps the Ca polyhedron. An additional cycle with a further 16H failed to adequately locate the OH groups, with 90% of the tests offering 8*f* and 8*g* positions that are likely to be oversymmetrical averages. These incomplete potential proton locations were then excluded from the model illustrated in Fig. 1, though we allowed the Ow occupancy to vary. This refines to occupancy = 0.900(13) (on 8*e*, *Z* = 2) and is equivalent to 3.60(21) H_2O and coincident with our independent analyses.

The resulting average structure is entirely consistent with that expected from a comparison with calumetite. However, and as discussed in Crichton and Müller (2017), there are a significant number of additional reflections that indicate *hkl*-dependent peak shape, specifically (*hk*0) reflections of a notionally doubled pseudotetragonal ($a = \sqrt{2}a_1$) lattice, with significant peak asymmetry, that can typically arise from stacking defects.

Table 3. Crystal data, data collection and structure refinement details.

Crystal data	
Crystal chemical formula	$Sr_{0.928(8)}Cu_4(OH)_6Cl_2{\cdot}3.60(21)H_2O$
Space group name	*Cmcm*
Space group number	63
Unit cell dimensions	
a (Å)	6.6791(6)
b (Å)	15.5006(6)
c (Å)	6.6811(6)
V (Å^3)	691.70(10)
Z	2
Density (diffraction) (g.cm^{-3})	2.842
Data collection	
Temperature (K)	293
2θ min–max (°)	2.166–26.952
Radiation (Å)	0.3999
h,*k*,*l* max	7, 18, 7
No. of reflections/parameters	345/47
Refinement	
R(reflections) (%)	$R = 7.96$, $R_{all} = 8.44\%$
Sigma weighted	w$R = 9.40\%$, w$R_{all} = 9.45\%$
R(profile)	$R = 16.49\%$, w$R = 22.74\%$
GoF	1.46

https://doi.org/10.1180/mgm.2021.66 Published online by Cambridge University Press

Table 4. Atom positions, occupancies and temperature factors.

Atom	Wyckoff	*x/a*	*y/b*	*z/c*	Occupancy	*U* (Å^2)
Cu	8*d*	¼	¼	0	1	0.008(4)
Cl	4*c*	½	0.1121(5)	¼	1	0.037(2)
Sr	4*c*	½	0.4110(3)	¼	0.464(4)	0.030(2)
O1 (OH)	8*g*	0.2045(18)	0.3049(10)	¼	1	0.097(10)
O2 (OH)	8*f*	0	0.1784(8)	0.0500(15)	1	0.005(5)
O3 (water)	8*e*	0.7555(19)	½	½	0.900(13)	0.047(4)

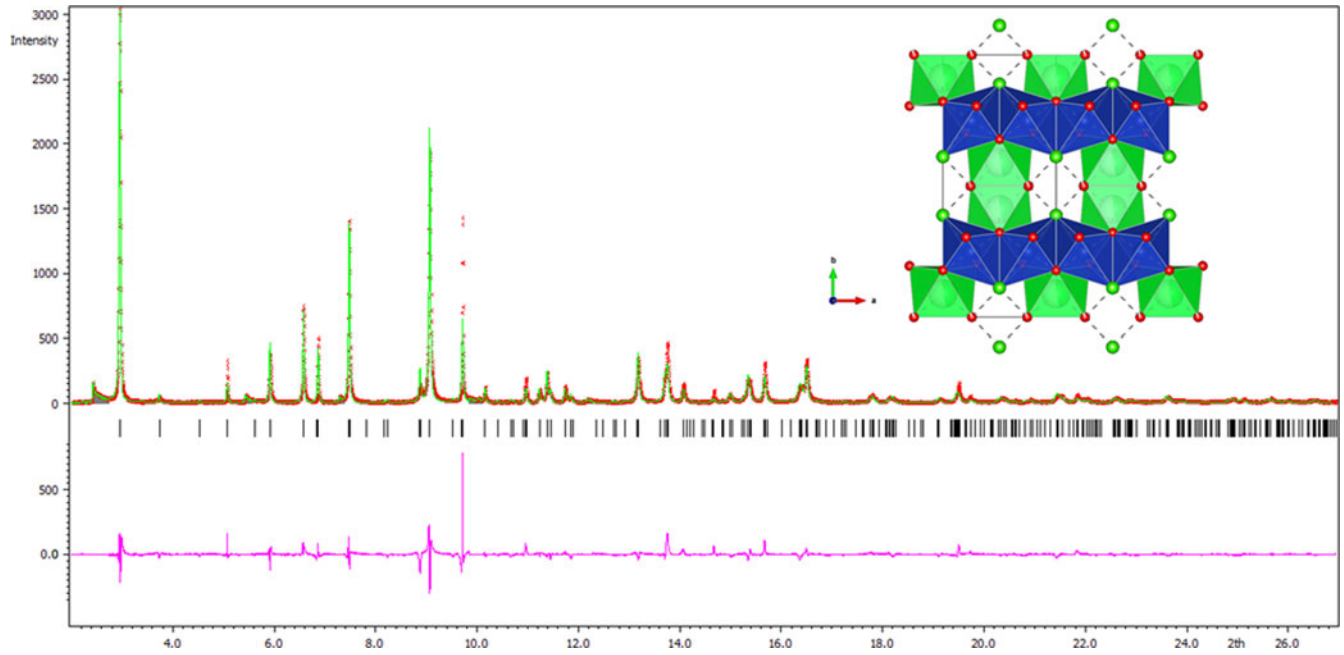

Fig. 1. Rietveld refinement of data from ID31 using Jana2006 against the model produced for **1** shown inset, using *Vesta* (Momma and Izumi, 2011). Excluded regions correspond to lattice doubled (*hk*0) positions.

Table 5. Selected bond and interatomic distances (Å).

Cu polyhedron	JT-distorted octahedron
Cu–O1 ×2	1.899(7)
Cu–O2 ×2	2.032(6)
Cu–Cl ×2	3.190(5)
Sr polyhedron	square antiprism
Sr–O1 ×2	2.567(14)
Sr–O2 ×2	2.434(7)
Sr–Ow ×4	2.760(8)
Ow environment	tetrahedron
Ow–Cl ×4	2.908(9)
Ow–Sr ×4	2.760(8)

Modelling structural disorder

Using the refined model as an illustration, it is straightforward to describe the same average structure in *DIFFaX+* (Leoni *et al.*, 2004) using one basis and a transition vector (TV) between the basis and its adjacent layer. In this case, in order to test easily accessible site- and the layer-ordering schemes, we only require that the basis represent the lower half of the average structure expanded to a $\sqrt{2} \times \sqrt{2}$ cell (+ lattice repeat; Fig. 2) and have changed the stacking direction to *z*. As a first step, we can simply investigate the effect of different stacking sequences of the basis to identify if the extra-average peaks and peak-shapes are reproduced by repeating an average structure basis at different locations above the previous, corresponding to edge-sharing, corner-sharing, or face-sharing adjacent Sr-polyhedra (Fig. 2).

The corner-sharing construction reduces, with symmetry search over a $2 \times 2 \times 12$ sample, to the basis, which may be Erdös *et al.*'s hemihydrate. The edge-sharing construction reduces to the average *Cmcm*, shared with calumetite and the face-sharing to an *I*-centred tetragonal structure of the same size, which bears more than a passing resemblance to the $Ba_2Cu_3O_4Cl_2$-type structure, well known to the superconductor community (e.g. Pitschke *et al.*, 1995). A comparison of these calculated ordered structures highlights their similarities and the location of characteristic peaks in the structures produced. In refining the different TVs that give rise to these stacking sequences, it is possible to introduce some degree of stacking disorder. While the result of this succeeds in reproducing a pattern equivalent to that produced by the average Rietveld refinement, it is no better. Inspection of the resulting probabilities indicates why: >99% of TVs produced are edge-sharing. A slightly defective stacking sequence of otherwise identical layers is not an efficient way of mirroring the defects in our observation. Another, perhaps additional, mechanism is required that allows for interlayer disorder without disrupting the intralayer stacking sequence significantly from average; i.e. edge-sharing. This is done, here, by ordering the ½-occupied Sr sites.

https://doi.org/10.1180/mgm.2021.66 Published online by Cambridge University Press

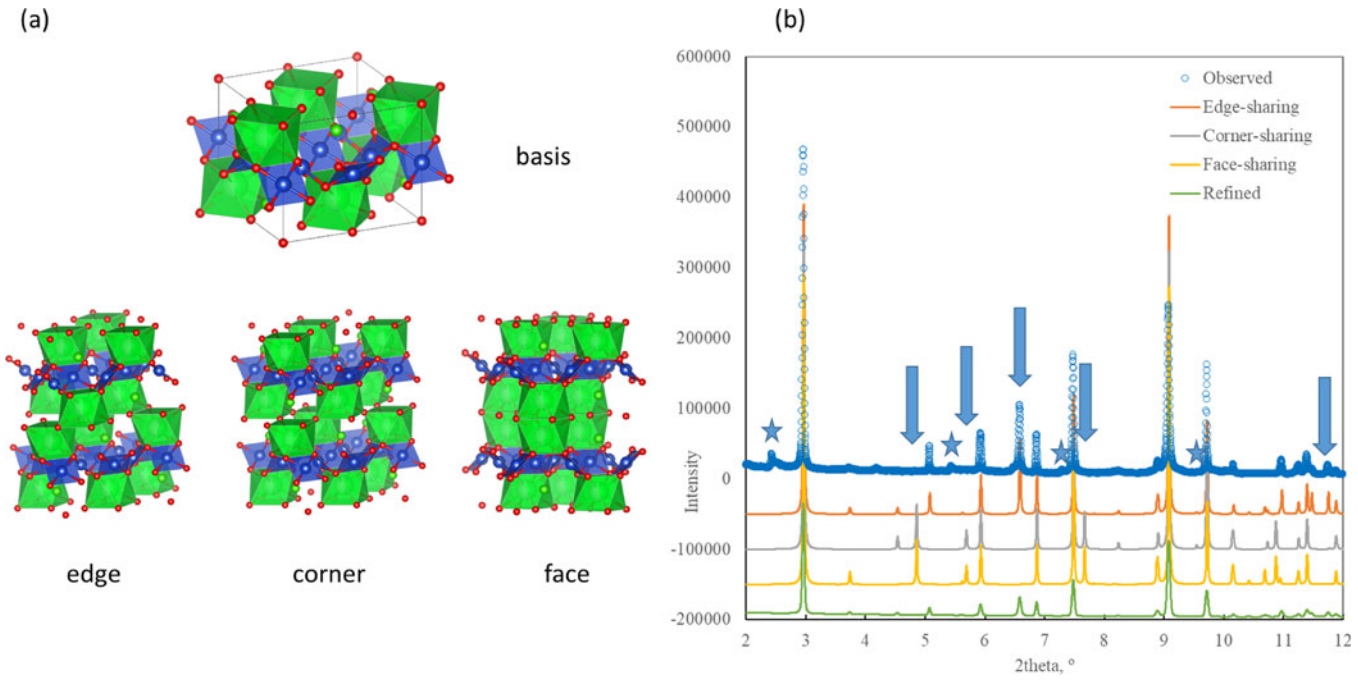

Fig. 2. (*a*) The basis is produced by halving the average structure over a doubled lattice. Adjacent layers may be combined with different TVs that give rise to edge-, corner- and face-sharing SrOH–H_2O polyhedral. Calculation of end-members and comparing these with the observed diffraction data (*b*) highlights the gross similarity of these models, their characteristic differences both between each other and with the observed (arrows) and their inability to fit those peaks characteristic of disordered layer structures (starred) when their probabilities are refined.

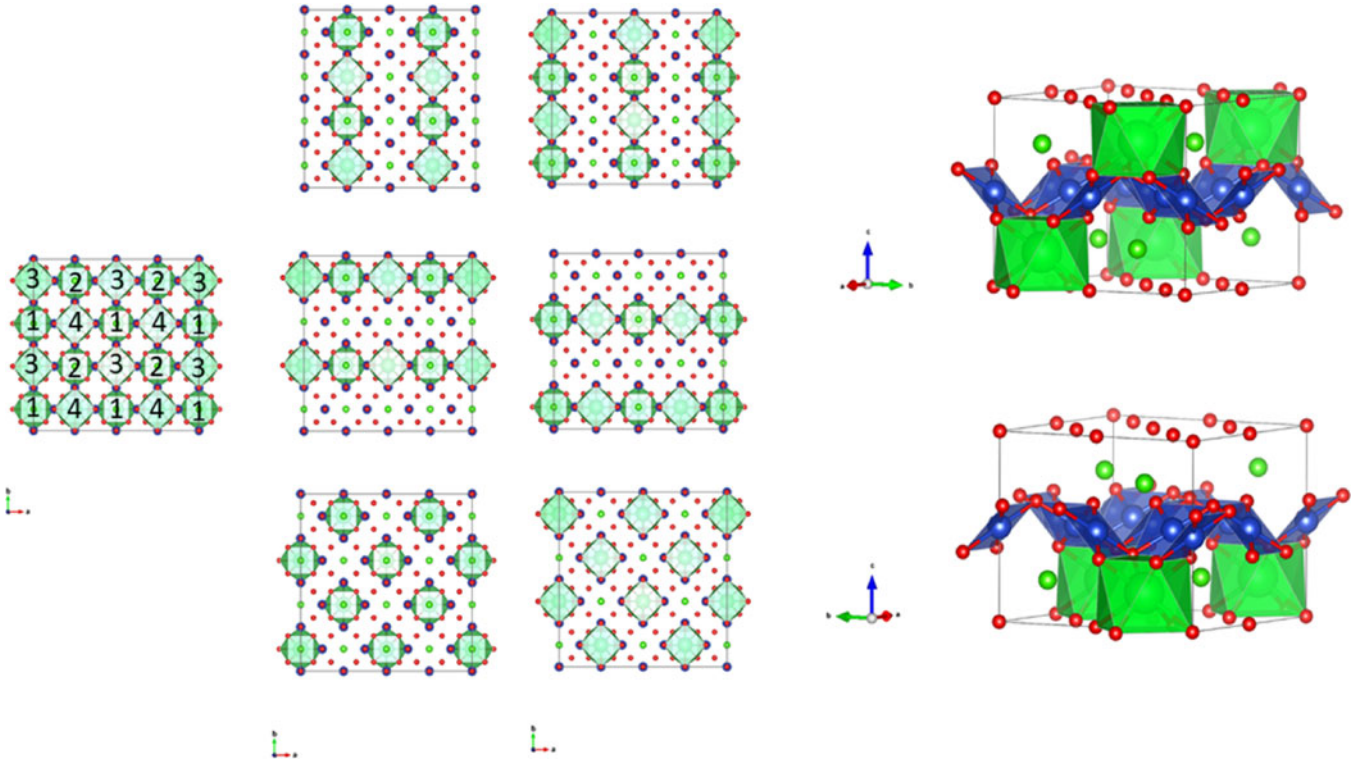

Fig. 3. Ordering over a $2a_1$, $2a_1$ lattice provides 6 bases that can be combined following the refinement of their populating probabilities to provide a model for site disorder (or Sr ordering within layers, for all other atoms are effectively constant), over the modelling of the diffraction intensities. These 6 layers reduce to two, which, if used, would provide for a more elegant model construction, in *Pnma* and *P*4*mm*.

Site ordering can occur in several (but limited) ways in the basis; the following illustrate six options for a revised series of layers, which retain layer chemistry but where the half the available Sr sites are fully occupied: in vertical (1, 3; 2, 4) distributions, in horizontal (1, 4; 3, 2), and diagonal bottom- (1, 2) and one top-occupied (3, 4) (Fig. 3). For the sake of simplicity, each

https://doi.org/10.1180/mgm.2021.66 Published online by Cambridge University Press

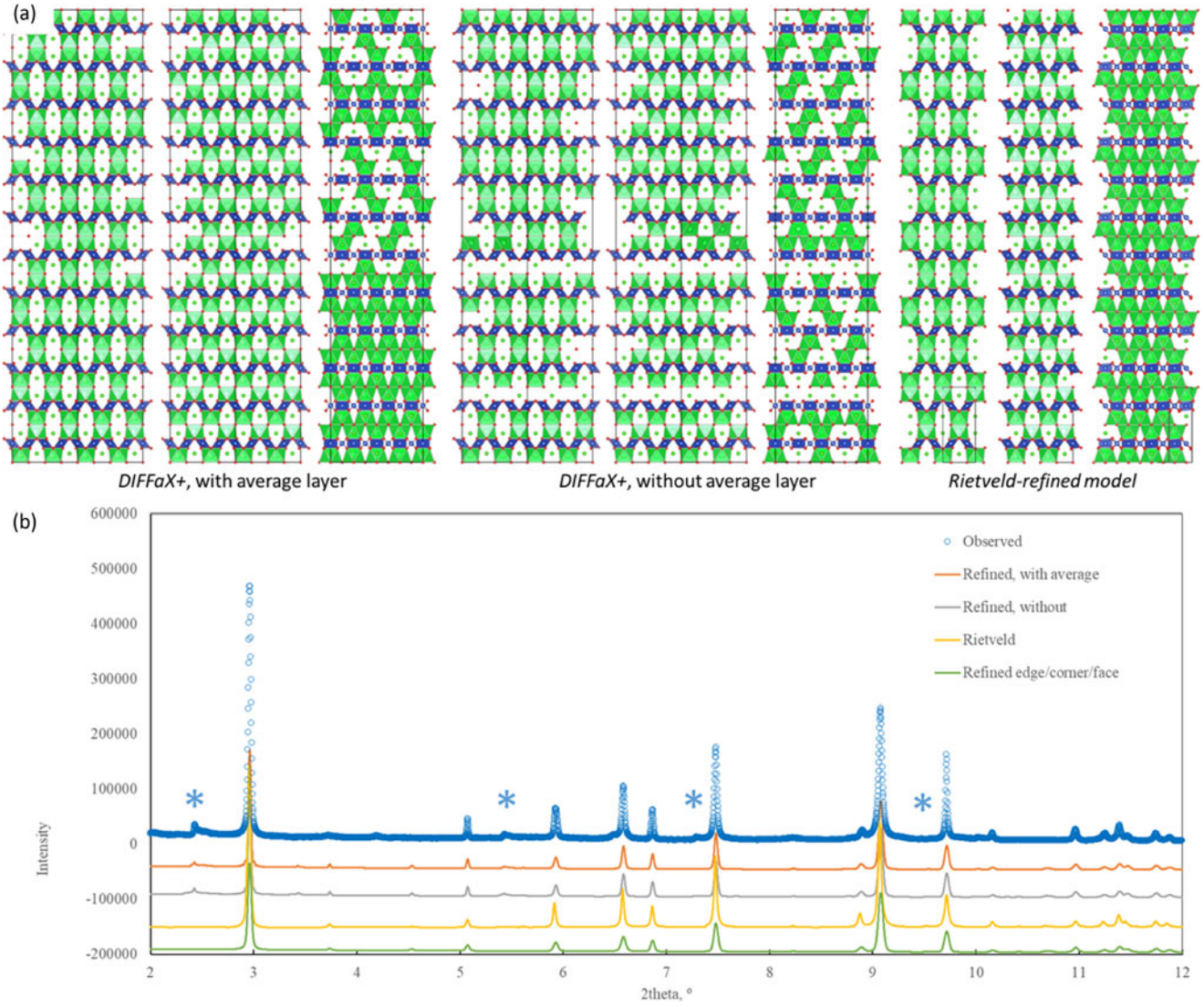

Fig. 4. (*a*) The refined structures of **1** following refinement of probability of Sr ordering schemes occurring in face-sharing arrangement, including the possibility of disordered layers (leftmost three, viewed along equivalent *a*, *c*, <110>), without (central three; available as crystallographic information files, deposited with the Principal Editor of *Mineralogical Magazine* and available as Supplementary material) and the Rietveld refined average structure (rightmost). These models are compared with the observed in part (*b*), showing from top, observed, with ordered model, with disordered allowed, without disordered layers in grey, followed by the Rietveld calculated pattern and, in green, the result of refining stacking sequences (edge-, corner- and face-sharing) average layers. The former pair and the latter pair produce equivalent fits with the former the only models that reproduce relevant intensities at the asterisked locations. The structure is therefore best modelled by stacking sequences of ordered layers in an edge-sharing arrangement, where the presence of some defective disordered layers does not degrade the fit quality.

layer has been chosen to have the same origin and any inherent symmetry has been removed. Other layers are of course possible by changing the total Sr per layer and other arithmetic constructions can be combined with layer rotation and full symmetrical descriptions to provide similar model solutions that are more elegant. This would reduce these 6 layers to two; in *P4mm*, $a \approx a_1$, $c = ½\ b_1$ Å and *Pmma*, $a \approx \sqrt{2}a_1$, $b \approx a$, $c = ½\ b_1$ Å, Fig. 3).

In this case, instead of varying the probabilities of an edge- face- or corner-sharing TV between otherwise identical layers, the TVs are identical (edge-sharing) and it is to a different occupancy pattern within layers that we affix the probabilities. That is, we effectively refine their population rather than how they commute. The sum will lead to a different Sr site order pattern, which will be determined only by minimising the difference between the diffraction patterns produced and that observed. The result is the following, shown in Fig. 4. Which is only a marginal improvement over the edge-sharing average above, but where, more importantly, it has reproduced intensities at lattice-doubled (110, 210, 320, etc) positions, including the generation of some asymmetry. A 2×2×12 layer snap-shot of part of the structure that produces this diffraction pattern looks like Fig. 4.

Similar constructions were also refined but without the inclusion of an average layer (all bases have ordered Sr). These result in an equivalent fit. Quite clearly elements of order are retained, where nearly no defects are visible in two of these images, viewed-off axis (Fig. 4a), left and centre of each group). However, any thoughts that there is no in-plane disorder is dispelled with an on-axis display (rightmost of each group). The disordering is in fact almost complete with no repeated sequence of identical layers along the stacking direction (equivalent to the *y* direction in the

https://doi.org/10.1180/mgm.2021.66 Published online by Cambridge University Press

Cmcm lattice). Refinement of probabilities of layer occurrence against diffraction data has, though, produced a hierarchical structure with local preferences (still limited only by diffraction) that creates local structures; the most common probabilities (>55%) give rise to a layer combination that sees sites 1,3|TV|1,4 and its opposite 2,4|TV|2,3 occupied, at 50% likelihood, 1,4|TV|1,4 and 2,3|TV|2,3; at 25% both 3,4|TV|1,2 and 1,2|TV|3,4 are equally probable. The latter pair, when isolated, reduce to a *Pmma* lattice; the former, to orthometric *C*2/*c* lattices at $\sqrt{2}a_1 \times b_1$, and the intermediate set to $P2_1/c$, the same size as the average, indeed the lattice that Crichton and Müller alluded to earlier. It is notable that none produce occupations that reproduce the average in a two layer sequence. At the next hierarchical level, the two highest probability layers will combine with the next pair; i.e. 1,3|TV|1,4|TV|1,4 and 2,4|TV|2,3|TV|2,3 to account for some 75% of all short-range structures starting from layers 1 and 2 and give the diagonal climb to the Sr occupation evident in the figures. That these two subunits form with equal probability, is testament to the pseudotetragonal lattice of the average. From the 12-layer structure produced, we can also demonstrate the validity of the overall average structure as a fair representative of this by rebinning the fractional positions by $z' = 12z\text{-int}(12z)$ and reducing c' to $c/12$. Such an operation reproduces the basis, itself derived directly from one half of the average structure. Evidently, as the diffraction pattern fits equivalently to, or even better than, the average Rietveld refinement, they are, at least, equivalent descriptions.

So what is the correct structure? These shown are only one potential model, many are possible from the recursively integrated intensities that are refined against the observed data. However, it is clear that the average crystallographic data is a fair representation of the average summation over the stacking direction. It appears the case that any disorder is highly directional and is caused by site ordering within layers as the principle source, here modelled only over Sr sites; and we recall that low-temperature refinements of centennialite also indicate disorder over Ca sites (Yoshida *et al.*, 2017). As alluded to earlier, the potential for steric issues abound in the anticipated H-bonding structure of the average, with (O)H atoms occupying the 8*f* and 8*g* sites, or split to nearby 16*h* positions, leading to short ½ occupied H–H distances. Ordering of these may also drive the inherent structural disorder. Whatever the mechanism, by this demonstration we are not required to alter the overall bulk chemistry significantly by introducing extra triply- or fully-vacant Sr layers, nor is there recourse to add any additional TV, or any Sr sites from those that control the construction of the average structure. When refined, it also appears that patterns are repeated that ensure that local features (and stoichiometry) are preserved and that ordering is very near complete in two axial directions.

Where the combination of local patterns differ from average, they may be separated and investigated to see if they are energetically favourable. These may be polytypes, polymorphs or other topological cousins with related chemistries, such as the hemihydrate of Erdös *et al.* (1981).

Comparing calumetite to a centennialite, a 'centennialite-(Sr)', should it exist, might be anticipated to have a similar lattice of $a \approx 6.67$ Å and a longer *c*-axis of $c \approx 6.08$ Å (given the proportionally longer Sr–Ow bonds), increasing the canting of Cu planes from the Sr–Cu–Sr plane. It seems likely then, from our survey and these considerations, that centennialites are limited to Ca and, possibly, Sr. From the proposed 'centennialite-(Sr)' lattice, and by using equivalent atomic positions, a first-order approximation of the *J* interactions can be nonetheless be calculated and synthesis targeted.

Conclusion

The Sr-equivalent of calumetite has been synthesised and its structure described, a description enabled by the investigation using *DIFFaX+* satisfies other features of the diffraction pattern of this phase and, in all probability, these can be transferred to the Ca analogue, calumetite. From elements of the structure contained herein, a first estimate of the structure of the 'Sr-centennialite' can be made.

Acknowledgements. Data presented here were collected at beamline ID31 during beamtime allocated to in-house research, we thank Prof. A. N. Fitch of the ESRF for making this available. Prof. P. Leverett and Dr. A. S. Askenov are thanked for their helpful and constructive reviews of the original manuscript.

Supplementary material. To view supplementary material for this article, please visit https://doi.org/10.1180/mgm.2021.66

References

Braithwaite R.S.W., Mereiter K., Parr W.H. and Clark A.M. (2004) Herbertsmithite, $Cu_3Zn(OH)_6Cl_2$, a new species, and the definition of paratacamite. *Mineralogical Magazine*, **68**, 527–539.

Crichton W.A. and H. Müller (2017) Centennialite, $CaCu_3(OH)_6Cl_2.nH_2O$, n~0.7, a new kapellasite-like species, and a reassessment of calumetite. *Mineralogical Magazine*, **81**, 1105–1124.

Dubler E., Vedani A. and Oswald H.R. (1983) New structure determination of murdochite, Cu_6PbO_8. *Acta Crystallographica*, **C39**, 1143–1146.

Erdös E., Denzler E. and Altorfer H. (1981) Thermochemical, crystallographic and infrared studies on calcium copper hydroxychloride hydrates. *Thermochimica Acta*, **44**, 345–361.

Feitknecht W. (1949) Über Doppelhydroxyde und basiche Doppelsalze. 7. Über basiche Doppelchloride des Kupfers. *Helvetica Chimica Acta*, **32**, 1653–1667.

Fitch A.N. (2004) The High Resolution Powder Diffraction Beam Line at ESRF. *Journal of Research of the National Institute for Standards Technology*, **109**, 133–142.

Iida K., Yoshida H.K., Nakao A., Jeschke H. O., Iqbal Y., Nakajima K., Ohira–Kawamura S., Munakata K., Inamura Y., Murai N., Ishikado M. Kumai R., Okada T., Oda M., Kakurai K. and Matsuda M. (2020) $q = 0$ long-range magnetic order in centennialite $CaCu_3(OD)_6Cl_2{\cdot}0.6D_2O$: A spin-perfect Kagome antiferromagnet with J_1–J_2–J_d. *Physical Review B*, **101**, 220408(R).

Jarek U., Holynska M., Slepokura K. and Lis T. (2007) Calcium chloride rhenate(VII) dihydrate. *Acta Crystallographica*, **C63**, i77–i79.

Kampf A.R., Sciberras M.J., Williams P.A., Dini M. and Molina Doloso A.A. (2013) Leverettite from the Torrecillas mine, Salar Grande, Iquique Province, Chile: the co-analogue of herbertsmithite. *Mineralogical Magazine*, **77**, 3047–3054.

Krause W., Bernhardt H.J., Braithwaite R.S.W., Kolitsch U. and Pritchard R. (2006) Kapellasite, $Cu_3Zn(OH)_6Cl_2$, a new mineral from Lavrion, Greece and its crystal structure. *Mineralogical Magazine*, **70**, 329–340.

Leoni M., Gualtieri A.F. and Roveri N. (2004) Simultaneous refinement of structure and microstructure of layered materials. *Journal of Applied Crystallography*, **37**, 166–173.

Lubej A., Koloini T. and Pohar C. (2004) Industrial precipitation of cupric hydroxyl-salts. *Acta Chimica Slovenica*, **51**, 751–768.

Malcherek T. and Schlüter J. (2007) $Cu_3MgCl_2(OH)_6$ and the bond-valence parameters of the OH–Cl bond. *Acta Crystallographica*, **B63**, 157–160.

Malcherek T., Bindi L., Dini M., Ghiara M. R., Molina Donoso A., Nestola F., Rossi M. and Schlüter J. (2014) Tondiite, $Cu_3Mg(OH)_6C_{l2}$, the Mg-analogue of herbertsmithite. *Mineralogical Magazine*, **78**, 583–590.

McQueen T.M., Han T.H., Freedman D.E., Stephens P.W., Lee Y.S. and Nocera D.G. (2011) $CdCu_3(OH)_6Cl_2$: A new layered hydroxide chloride. *Journal of Solid State Chemistry*, **184**, 3319–3323.

Miyawaki R. Hatert F., Pasero M. and Mills S.J. (2019) IMA Commission on New Minerals, Nomenclature and Classification (CNMNC) NEWSLETTER

49: New minerals and nomenclature modifications approved in 2019. Proposal 18–C. *Mineralogical Magazine*, **83**, 479–483.

Momma K. and Izzumi F. (2011) VESTA 3 for three-dimensional visualization of crystal, volumetric and morphology data. *Journal of Applied Crystallography*, **44**, 1272–1276.

Nishio-Hamane D. Momma K., Ohnishi M., Shimobayashi N., Miyawaki R., Tomita N., Okuma R., Kampf A. R. and Minakawa T. (2017) Iyoite, $MnCuCl(OH)_3$ and misakiite, $Cu_3Mn(OH)_6Cl_2$: new members of the atacamite family from Sadamisaki Peninsula, Ehime Prefecture, Japan. *Mineralogical Magazine*, **81**, 485–498.

Oswald H. R. and Feitknecht W. (1964) Über Hydroyhalogenide $Me_2(OH)_3Cl$,-Br,-J zweiwertiger Metalle (Me=Mg,Ni,Co,Cu,Fe,Mn). *Helvetica Chimica Acta*, **47**, 272–289.

Petříček V., Dušek M. and Plantinus L. (2014) Crystallographic computing system JANA2006: General features. *Zeitschrift für Kristallographie*, **229**, 345–352.

Pitschke W., Krabbes G. and Mattern N. (1995) Powder diffraction data and Rietveld refinement of the compound $Ba_2Cl_2Cu_3O_4$. *Powder Diffraction*, **10**, 282–287.

Putz H., Schoen J.C. and Jansen M. (1999) Combined method for "ab initio" structure solution from powder diffraction data. *Journal of Applied Crystallography*, **32** 864–870.

Schlüter J., Malcherek T., Pohl D. and Schäfer C. (2019) Vondechenite, a new hydrous calcium copper chloride hydroxide, from the Bellerberg, East–Eifel volcanic area, Germany. *Neues Jahrbuch Mineralogische Abhandlungen*, **195**, 79–86.

Sun W., Huang Y.X., Pan Y. and Mi J.X. (2016) Synthesis and magnetic properties of centennialite: a new S = ½ Kagome antiferromagnet and comparison with herbertsmithite and kapellasite. *Physics and Chemistry of Minerals*, **43**, 127–136.

Williams S.A. (1963) Anthonyite and calumetite, two new minerals from the Michigan copper district. *American Mineralogist*, **48**, 614–619.

Yoshida H., Noguchi N., Matsushita Y., Ishii Y., Ihara Y., Oda M., Okabe H., Yamashita S., Nakazawa Y., Takata A., Kida T., Narumi Y. and Hagiwara M. (2017) Unusual magnetic state with dual magnetic excitations in the single crystal of S = ½ kagome lattice antiferromagnet $CaCu_3(OH)_6Cl_2.0.6H_2O$. *Journal of the Physical Society of Japan*, **86**, 033704.

https://doi.org/10.1180/mgm.2021.66 Published online by Cambridge University Press